Fundamentals of Au(111) Surface Dynamics: Coarsening of 2D Au Islands

Peter M. Spurgeon,[a] King C. Lai,[b,c] Yong Han,[b,c] James W. Evans,[b,c,*] and Patricia A. Thiel[a,c,d,*]

[a]Department of Chemistry, Iowa State University, Ames, Iowa 50011 USA
[b]Department of Physics & Astronomy, Iowa State University, Ames, Iowa 50011 USA
[c]Ames Laboratory, USDOE, Ames, Iowa 50011 USA
[d]Department of Materials Science & Engineering, Iowa State University, Ames, Iowa 50011 USA

ABSTRACT

Au(111) surfaces play a central role in many applications, yet studies of fundamental aspects of their dynamics are limited. Thus, using Scanning Tunneling Microscopy (STM) at 300 K, we analyze the coarsening of first-layer 2D Au islands directly on the Au(111) substrate, and also of second-layer 2D Au islands. Specifically, we monitor the decay of Au first-layer islands with areas of about 100-500 nm^2 in the vicinity of larger islands or extended step edges over a period of approximately 40 hours - the relevant time scale for this process. Experimentally observed behavior is captured by analytic theory for terrace-diffusion-limited decay incorporating DFT results for the Au terrace diffusion barrier and the adatom formation energy. Experimental observations of second layer island decay were also compared with appropriate analytic theory and stochastic simulations, thereby determining the effective Ehrlich-Schwoebel barrier for Au on Au(111).

1. INTRODUCTION

The importance of and interest in Au(111) surfaces derives from their role in diverse applications. One of these is the well-recognized use of Au(111) as a substrate for self-assembled monolayers.[1-3] The interaction between sulfur-containing head groups and the surface of gold is central to anchoring and ordering of organic molecules, especially alkanethiols and their derivatives, on Au(111). In another application area, Au(111) surfaces are effective catalysis for various surface reactions including selective oxidation and oxidative coupling, formation of methyl acrylates, etc.[4,5] In this context, it should be noted that the Au surface is not necessarily static or frozen under chemisorption or reaction environments, but rather can be dynamic or fluxional.[6,7] In a third application, Surface Enhanced Raman Spectroscopy (SERS) has traditionally exploited rough nanostructured (111) surfaces of Au and Ag, where relaxation of such morphologies has a significant impact on sensitivity.[8]

In addition, currently 3D Au nanoparticles (NPs) are used extensively for various applications. These include SERS and more generally plasmonics,[9,10] biosensing and medical imaging,[11-13] and catalysis.[14,15] In this context, we note that the equilibrium Wulff shape of such NPs in the larger size regime where they have crystalline fcc structure is dominated by (111) facets.[16,17] Also, synthesis of smaller NPs often produces truncated octahedral growth shapes with prominent (111) facets.[18] NPs are intrinsically metastable, and for all these applications resistance to coarsening (often called ripening or sintering) is critical. Degradation of supported metal catalyst NPs is typically associated with this phenomenon.[19] Although it is not the focus of the current study, analysis of surface-diffusion mediated reshaping of three-dimensional (3D) Au NPs synthesized with non-equilibrium growth shapes,[20] or of coalescence of pairs of NPs,[21]

requires precise characterization of surface diffusion on (111) and other facets. Fundamental studies of diffusion processes on extended single crystal surface are thus invaluable in providing the input to achieve predictive modeling of such processes.[22,23]

One class of fundamental studies of surface diffusion dynamics in metal homoepitaxial systems explores the coarsening of arrays of two-dimensional (2D) islands in the submonolayer coverage regime under ultra-high vacuum (UHV) conditions. Coarsening is driven by the reduction of the free energy cost associated with the cluster edges. Such processes in homoepitaxial systems constitute the 2D analogue of coarsening of 3D supported metal NPs mentioned above in the context of catalyst degradation. There are extensive studies of such coarsening processes for (111) surfaces of Ag and Cu, as summarized in reviews,[24-26] in contrast to Au. For extended surfaces with broad terraces and large arrays of 2D islands, coarsening kinetics can be quantified by tracking the decrease in the number of clusters and an increase in their mean size over time. There are two coarsening mechanisms, Ostwald Ripening (OR) and Smoluchowski ripening (SR). SR involves diffusion and coalescence of islands, while OR, the more common of the two, involves a transfer of metal across the surface from smaller clusters to larger clusters. OR dominates on (111) surfaces of Ag and Cu, in contrast to (100) surfaces,[25] and the same might be expected (and is observed in this study) for Au.

For narrow terraces, where islands are often located nearby extended steps, or for observations tracking only a few islands, a more appropriate alternative strategy to characterize coarsening kinetics is to track changes in individual island areas with respect to time.[24-28] The decay of smaller than average metal islands under OR, which can occur on the time scale of seconds to days, can be monitored in real time with Scanning Tunneling Microscopy (STM). This approach is used in the current study.

As an extension to the above studies, it is natural to also consider relaxation processes in multilayer homoepitaxial films, i.e., smoothening processes. Note that experiments are performed well below the thermal roughening transition, so that the metal surface has a smooth equilibrium morphology. Deposition in the presence of an additional Ehrlich-Schwoebel (ES) barrier for downward interlayer transport (relative to intralayer transport) results in kinetic roughening manifested by the formation of mounds (i.e., multilayer stacks of 2D islands).[29,30] Relaxation results in the decay of higher-layer islands, a process which is inhibited by the ES barrier. Thus, analysis of such decay processes produces an estimate of the ES barrier, a feature which we exploit in the current study for Au(111). Such analysis was first performed for Ag(111),[31] where the ES barrier was also assessed independently by analysis of film growth morphologies.[32] As an aside, it is not clear that Density Functional Theory (DFT) can currently provide values for such barriers which are sufficiently reliable to precisely describe, e.g., kinetically roughened film growth morphologies.[30]

Finally, we note that there exist previous UHV STM-based studies of Au(111) surface dynamics at room temperature. In fact, a prominent early study was presented as the first direct STM observation of surface self-diffusion on metals.[33] In this case, a controlled STM tip touch generated multi-level vacancy pits on the surface with size of a few thousand (missing) atoms, the filling of which is monitored at 300 K. Another study produced features on the Au(111) surface by sputtering with Ar, and observed "negligibly slow" decay rates for islands and pits at 300 K over 12.5 hours.[34] They determined an upper limit for the decay of vacancy islands of 0.18 nm^2/min, but did not report any decay rates for adatom islands. Our observations based upon monitoring surface evolution over about 40 hours quantifies decay rates for islands under UHV conditions at 300 K which are comparable to this upper limit. Exposure of the Au surface to

atmosphere was found to significantly enhance decay rates,[34] a feature analyzed more systematically for other coinage metals.[23,35] Another study considered the thermal annealing of Au thin films on mica, including analysis of the decay of 2D islands above room temperature.[36] The effect of the herringbone reconstruction of clean Au(111) surface was not considered in these analyses, and will also not be considered in our treatment.

In Sec.2, we describe our experimental and theoretical methodology. Experimental results are presented in Sec.3, and theoretical analysis and modeling in Sec.4. Comparison of the observed behavior for Au(111) with that for Ag(111) and Cu(111) is provided in Sec.5. Conclusions are provided in Sec.6.

2. METHODS

2.1. Experimental details

All experiments were carried out in a stainless-steel ultrahigh vacuum (UHV) chamber with a base pressure of 2 x 10^{-10} Torr, equipped with an Omicron variable temperature STM (VT-STM). A single crystal of Au(111) was cleaned via Ar^+ sputtering (I_S = 8 – 12 μA, 2 kV, 5 - 10 min) and annealing (500K, 10 - 15 min) cycles. These cycles were carried out until no impurities were detected by Auger electron spectroscopy (AES). A coverage of 0.3 monolayers (ML) of Au was deposited (*Flux* = 5 ×10^{-3} ML/s, 1 min deposition time) onto the sample via an Omicron EFM3 UHV metal evaporator with the sample held at room temperature. Au island coverage was determined using WsXM software, in which terrace images were flooded to give the proportion covered by islands.

The XY (in-plane) piezoelectrics were calibrated against the (7 × 7)-Si(111) reconstruction on a Si(111) substrate. The Z (vertical) calibration was checked by analysis of steps on Au(111) which have a nominal height of 0.236 nm.[37] Typical tunneling current (I) was 1.0 nA, with sample biases, V_S, of 1.0 V. A PtIr STM tip was used which was cleaned via pulsing to $|V_S|$ = 5 - 10 V for several minutes to hours over the Au surface until the Au(111) herringbone reconstruction was readily imaged over multiple images. A drift correction in the MATRIX software was enabled so one area could be imaged repeatedly over many hours.

2.2. Analytic theory for island evolution

The traditional formulation considers the evolution (growth or shrinkage) of a specific first-layer island of radius R in an array of other first layer islands which are described within an effective medium framework.[23-26,38,39] Atoms detach and reattach from island edges and diffuse across the surface. The density of adatoms diffusion across on the surface is denoted by ρ. We assume that there is no additional barrier for lateral attachment of atoms to island edges, as is confirmed by experiment, corresponding to terrace-diffusion (TD) limited OR. This implies the boundary condition $\rho = \rho^{eq}(\infty)\, e^{\left(\frac{\gamma\Omega}{k_B T R}\right)}$, based upon the Gibbs-Thompson relation, for the equilibrated adatom density at the edge of the island of radius R. Here, γ denotes the step energy per unit length, Ω denotes the area of the surface unit cell, k_B denotes Boltzmann's constant, and T denotes the surface temperature. The array of other islands is described by imposing a boundary condition $\rho = \rho^{eq}(\infty)\, e^{\left(\frac{\gamma\Omega}{k_B T R_C}\right)}$ on an outer boundary with radius L_c, where R_c denotes the mean radius of nearby islands. See Fig.1. The choice of L_c is discussed later. It is common to select $(R_c/L_c)^2 = \theta$, the specified island coverage, so then L_c reflects the mean island separation,

although in some cases we make a different choice. Also, $\rho^{eq}(\infty) = \exp[-E_{form}/(k_BT)]$ is the equilibrium adatom density at an extended straight step in dimensionless units of atoms per surface unit cell, corresponding to $R = \infty$. Also, E_{form} denotes the adatom formation energy, corresponding to the total lateral interaction energy in an extended overlayer or island. Analysis of the above boundary-value problem (BVP) for the diffusion equation for ρ in the steady-state regime yields determines the net flux of attaching/detaching atoms at the perimeter of the specific islands, which in turn determines the evolution of its radius via

$$\frac{\partial R}{\partial t} = \frac{D_{TD}}{R}\rho^{eq}(\infty)\left[e^{\left(\frac{\gamma\Omega}{k_BTR_C}\right)} - e^{\left(\frac{\gamma\Omega}{k_BTR}\right)}\right]\left[ln\left(\frac{L_C}{R}\right)\right]^{-1}, \qquad (1)$$

where D_{TD} is adatom terrace diffusion coefficient. Then, R(t) is determined by numerical integration of (1) where R(t=0) corresponds to the experimental initial size.

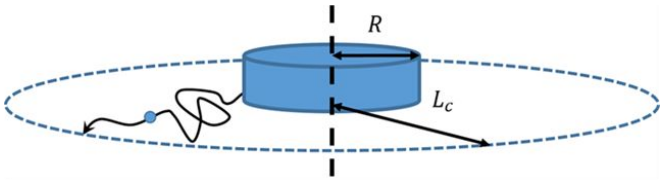

Figure 1. *Schematic of the geometry used for analysis of diffusion-limited decay of a first-layer island with radius R. An outer boundary condition is imposed at radius L_C reflecting the feature that the mean radius of nearby islands is R_C.*

Decay of second-layer islands of radius R is treated by similar approach but with a different boundary condition at the edge of the supporting island of radius R_S (with the second-layer island assumed to be centrally located). See Fig. 2. Let r denote the radial distance from the island center. Then, the presence of an ES barrier, δ, inhibiting downward transport, one has that[23-25,39] $\partial\rho/\partial r = [\rho - \rho^{eq}(\infty)]/L_\delta$ for $r = R_S$ for ES attachment length, $L_\delta = a(e^{(\delta/(k_BT))} - 1)$, where a = 0.289 nm is the Au surface lattice constant. Solving the appropriate BVP for steady-state diffusion equation determines the evolution of the radius of the second layer island via

$$\frac{\partial R}{\partial t} = \frac{D_{TD}}{R}\rho^{eq}(\infty)\left[e^{\left(\frac{\gamma\Omega}{k_BTR_S}\right)} - e^{\left(\frac{\gamma\Omega}{k_BTR}\right)}\right]\left[ln\left(\frac{R_C}{R}\right) + \frac{L_\delta}{R_S}\right]^{-1}. \qquad (2)$$

R(t) is determined by integration of (2) with the experimental values of R(t=0) and R_S.

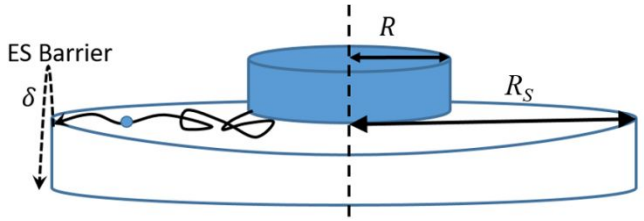

Figure 2. *Schematic of the geometry used for analysis of diffusion-mediated decay of a second-layer island with radius R supported on a first-layer island of radius R_S.*

2.3. DFT and other analysis of energetics, stochastic modeling, KMC simulation

Previous analyses of the terrace diffusion barrier for Au on Au(111) included estimates of E_d = 0.12-0.14 eV using a Tight Binding-SMA potential,[40] E_d = 0.20 eV from DFT LDA and E_d = 0.15 eV from GGA-XC,[41] and more recently E_d = 0.12 eV from GGA-PW91.[42] See Ref. 43 for a more comprehensive listing of previous theoretical analyses including early results from lower-level semi-empirical treatments. There are no experimental estimates for E_d. Our own DFT analysis used a 5 layer Au slab, a 5×5 lateral unit cell (so that the Au(111) surface in this analysis is unreconstructed), and a 9×9×1 k-mesh with energy cutoff of 400 eV. Using the PBEsol functional, our Nudged Elastic Band analysis obtained E_d = 0.125 eV. From analysis of the energetics of a complete Au layer on Au(111), one obtains a total energy per Au surface atom of 3.925 eV. Together with the knowledge of the adsorption energy, E_{ad} = 3.138 eV, for an isolated Au atom, one obtains a value for the lateral interaction energy of Au atoms in a complete layer which corresponds to the formation energy of an Au adatom of E_{form} = 0.787 eV. Previous additional rough analysis indicated edge diffusion barriers in the range, E_e = 0.35-0.45 eV,[23] and our analysis with a 5×5 unit cell finds higher values of E_e = 0.43-0.55 eV. However, the E_e are not critical parameters for the current analysis which instead is sensitive to E_d, E_{form}, and γ.

A stochastic lattice-gas model was implemented for island decay, and specifically applied to assess fluctuations in second-layer island decay. The model assumes effective nearest-neighbor attractive lateral interactions between adatoms of strength $\phi = E_{form}/3 = 0.26$ eV. Since in this model, each atom in a complete surface layer has six shared NN interactions, this recovers E_{form} listed above. It also follows that the step energy satisfies $\gamma = \phi/a = 0.26$ eV/a. Atoms hop to NN empty sites with Arrhenius rate $h = \nu \exp(-E_{act}/(k_B T)]$, where the choice of E_{act} must be consistent with detailed-balance. Again, T denotes the surface temperature, and k_B is Boltzmann's constant. For terrace diffusion and attachment-detachment at island edges, we select $E_{act} = E_d - E_i (+ \delta)$, where $+\delta$ is included only for interlayer transport. For edge diffusion, we select $E_{act} = E_e - (E_i - E_f)/2$. Here $E_{i(f)} = -n_{i(f)} \phi$ is the lateral interaction energy for the adatom before (after) hopping. We set E_d = 0.125 eV, E_e = 0.35 eV and regard the ES barrier, δ, as a free parameter. Model behavior was analyzed via Kinetic Monte Carlo (KMC) simulations which implements various hopping processes with probabilities proportional to the physical rates.

As an aside, we note that the terrace diffusion coefficient is given by $D_{TD} \sim a^2 \nu \exp[-E_d/(k_B T)]$. As a result, based on Eq. 2, the effective energy barrier for coarsening in the absence of an attachment barrier is given by $E_{OR}(\text{Au}) = E_d + E_{form} = 0.91$ eV for Au islands on Au(111). This result neglects a contribution which depends on typical island size or curvature,[44] but this contribution is typically small.

3. EXPERIMENTAL RESULTS

3.1. Evolution of first-layer islands

Fig 3. shows a sequence of STM images of Au islands on Au(111) from t = 40 min to t = 2384 min, where t represents the time since island formation by Au deposition. The majority of islands are in the first layer, with a few generally smaller second-layer islands. Second layer island decay is discussed in Sec. 3.2. Apart from one very small island and one large partly

coalesced pair, first-layer island sizes are in the range of approximately 100 - 1000 nm^2. Throughout the 2384 min observation period, some islands undergo reshaping towards the preferred equilibrium structure. Restructuring and reshaping of islands are discussed elsewhere.[23]

Apart from the very small island at the top of the first image which quickly disappears, four other "smaller" islands with initial sizes from 90-400 nm^2 were observed to fully decay (colored circles in Fig. 3). The island in the white dashed circle does fully decay, but due to tip drift the island shifted partly out of the field of view so its decay was not tracked. All the islands decay via Ostwald Ripening, as confirmed by the observed gradual decrease of the island area over time. For the four islands circled in multiple colors, three of the islands are located next to an extended step edge, while the island circled in gray is further away from that step edge and surrounded by substantially larger islands. The island areas decay with time in a non-linear fashion as shown in Fig. 4 consistent with TD-limited OR. The color coding in Fig. 4 matches that in Fig. 3. The initial decay rate of the first layer Au islands is roughly 0.08 ± 0.02 nm^2/min and the rate increases during the late stages of decay.

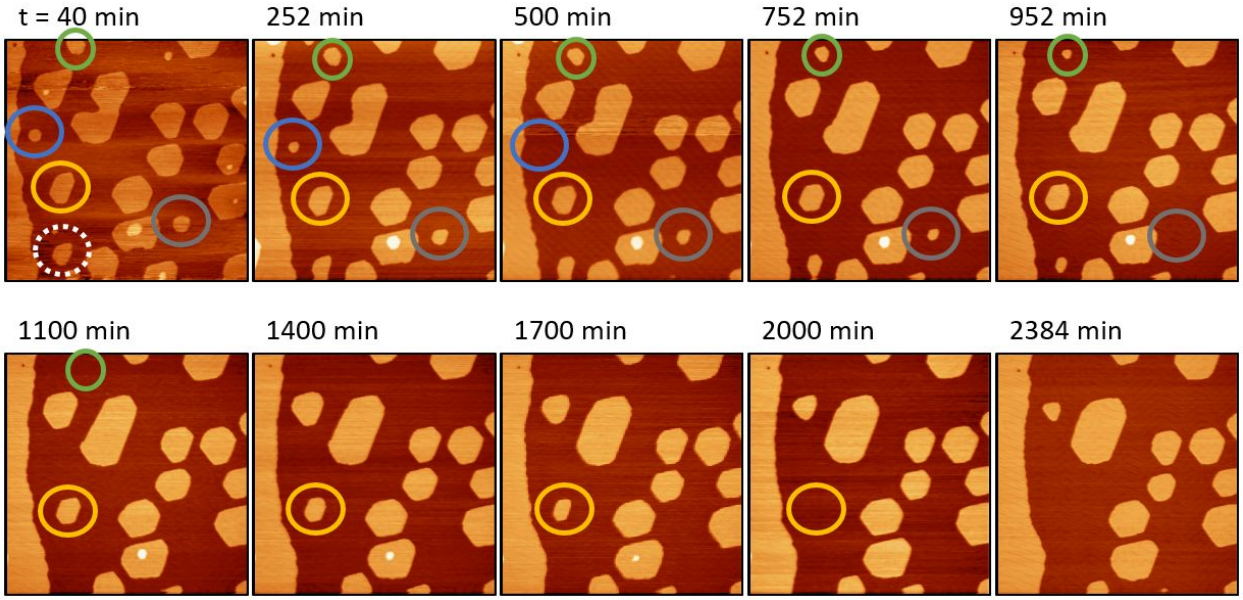

Figure 3. *STM images showing the coarsening of 2D Au islands on an Au(111) substrate from t = 0 min to t = 2384 min. Colored circles in the STM image are around islands that fully decay. All images are 200 x 200 nm^2, I = 1.0 nA, V_S = 1.0 V.*

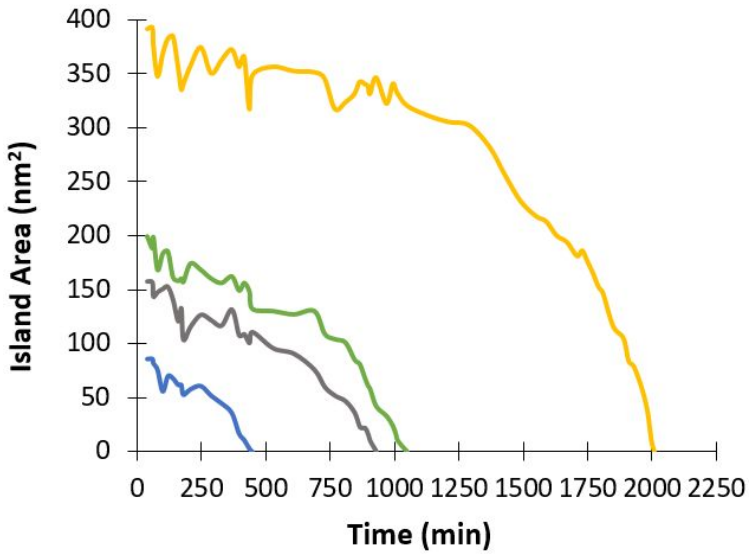

Figure 4. *Island area versus time for the four islands that are circled in Fig. 3. The color coding matches that in Fig. 3*

Next, we provide two additional examples of behavior reflecting TD-limited OR kinetics where island decay shows a sensitivity to the local environment. First, consider the "medium" sized island circled in blue in Fig. 5, located next to a step edge, which shows partial decay. When the smaller neighboring island circled in green disappears, the decay rate of the island circled in blue increases, a signature of TD-limited kinetics.[24-27] Second, Fig. 6 compares two initially similar sized islands at different locations. One is right next to the step edge, and the other is further away and is surrounded by multiple islands of a similar size. The island next to the step edge (blue circle) exhibits area decay, while the island further away (black circle) shows a slight increase in area. Islands next to step edges are expected to decay more rapidly since the extended step is a more effective sink for diffusing atoms having lower chemical potential than finite sized islands.

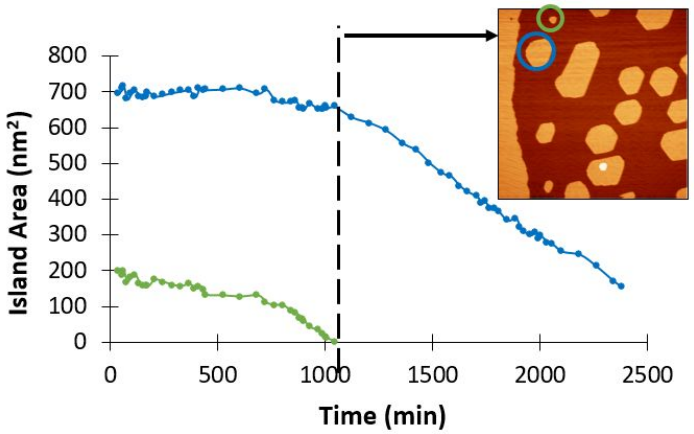

Figure 5. *Island area versus time for two nearby islands. The dashed line shows the time at which the island circled in green has disappears, after which the larger island circled in blue starts to decay. STM insert shows the two islands that were monitored.*

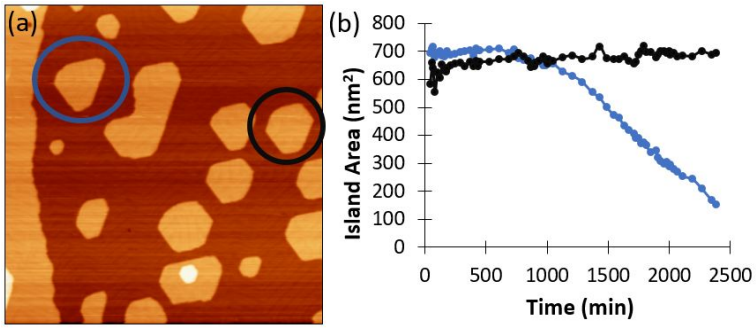

Figure 6. *(a) STM image of Au islands on Au(111) at t = 252 min. (b) Island area versus time comparing two islands of similar size. The black (blue) curve corresponds to the island that is circled in black (blue) in Fig. 6a.*

3.2. Decay of second-layer islands

Fig.3 provides one example of a decaying second-layer island appearing in the lower portion of the STM images. However, the shape of the supporting first-layer island appears anomalous perhaps due to the influence of a defect in the substrate. Specifically, the lower edge is initially severely indented, in contrast to the quasi-hexagonal equilibrium shape, although this indentation does heal over time. Thus, we performed additional experiments to find a more conventional example shown in Fig. 7, which presents a sequence of STM images of a second-layer island decay from t = 47 min to t = 1303 min. The second-layer island has an initial area of 170 nm^2. It is located slightly off center of the supporting island which has an initial area of roughly 1350 nm^2 increasing to about 1600 nm^2 over the observation period. The areal increase of around 250 nm^2 is larger than the initial area of the second-layer island. The feature that the increase in area of the supporting island exceeds the total area of the second-layer island (which decays transferring all of its atoms to the supporting island) reflects the scenario wherein other nearby smaller islands on the substrate also decay transferring atoms to the supporting island. The observed decay of the second-layer island is quantified below in Sec.4.1.

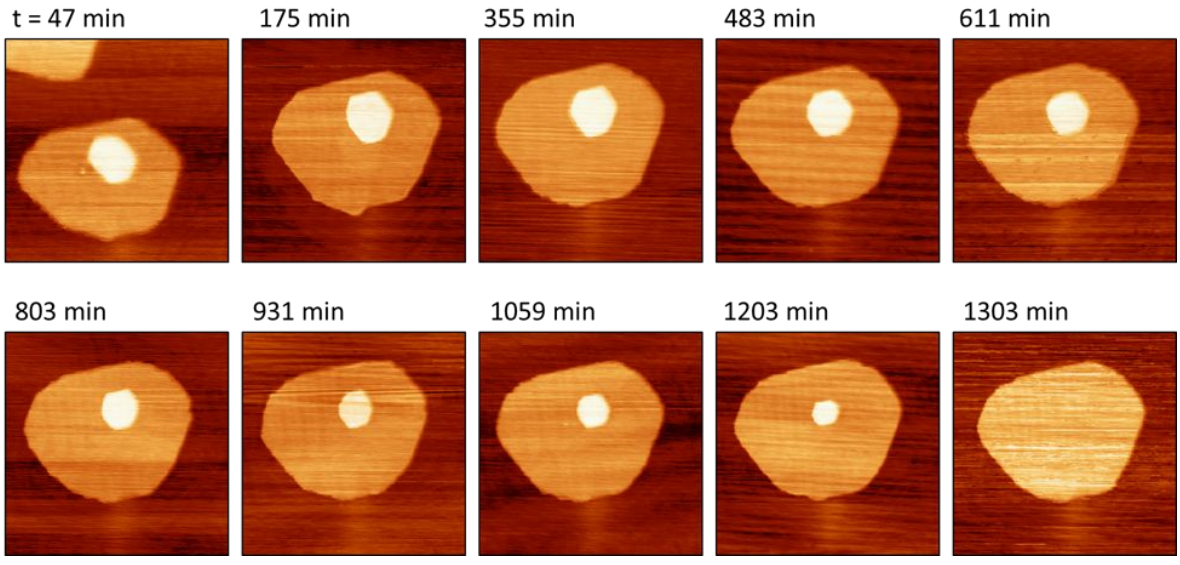

Figure 7*. STM images showing second-layer island decay over the course of 1303 min. Image area 67 x 67 nm^2, I = 1.0 nA, V_S = 1.0 V.*

Fig. 8 compares the decay of area of the second-layer island (blue line) shown in Fig.7 with that of a first-layer island (red line) of a similar size. The first-layer island is not located next to a step edge, but is surround by larger islands of comparable size to the supporting island in Fig.7. The second-layer island fully decays in 1303 minutes, while the first-layer island fully decays in 928 minutes. A second-layer island is expected to decay more slowly than the first-layer island due to the presence of the ES barrier at the edge of the supporting island.

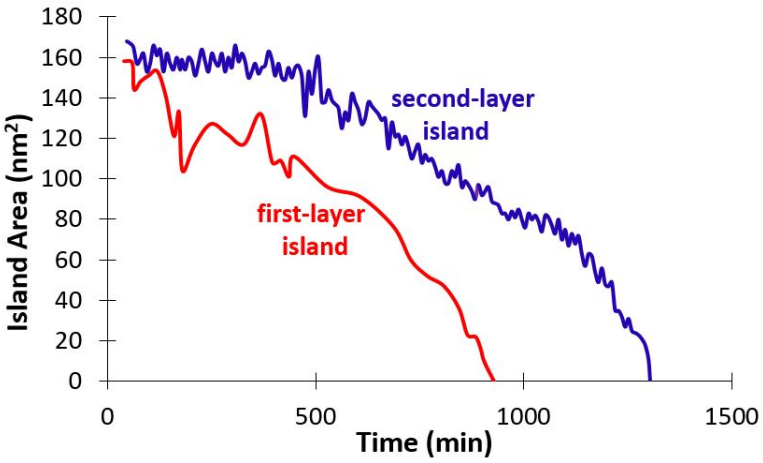

Figure 8. *Island area versus time examining the decay of similarly-sized first-layer (red) and second-layer (blue) islands. Note that individual data points, which are sparser for the first-layer island than for the second-layer island, are not shown individually, but instead are joined by smooth curves.*

4. THEORETICAL ANALYSIS

4.1. Analytical modeling of the decay of first- and second-layer islands

For first-layer islands, $R(t)$ versus t was determined for the four islands tracked in Fig.3 and Fig.4 from numerical integration of Eq. 1 with the experimental initial sizes, $R(t=0)$. We choose parameters $\nu = 10^{13}$/s and $E_d = 0.125$ eV determining D_{TD}, together with $E_{form} = 0.76$ eV and $\gamma = 0.865$ eV/nm guided by DFT results described in Sec.2C, $T = 300$ K, and $\Omega = (\sqrt{3}/2)a^2 = 0.0723$ nm^2. For islands away from the step edge we choose $R_C = 56$ nm, and set $L_C = \theta^{-1/2} R_C$ with $\theta = 0.3$ ML. This applies for just one of the tracked islands, specifically the one with initial size $R(t=0) = 24.7$ nm and initial area 155 nm^2 (purple curve in Fig.9). For the other three islands close to the extended step, it is more natural to choose L_C to reflect the distance of the island from the step ($L_C = 40$, 17, and 35 nm for islands with $R(t=0) = 27.7$, 18.6, and 38.6 nm indicated in green blue, and yellow, respectively). R_C is assigned a very large value for these islands reflecting the strong adatom sink provided by the extended step (and behavior is not sensitive to this value $R_C \approx 300\ R(t=0)$ as $e^{\left(\frac{\gamma\Omega}{k_B T R_C}\right)} \approx 1$). Fig. 9 compares the calculated decay of islands (solid lines) with the experimental data (dashed lines).

The analytical modeling matches reasonably well experimental behavior for the larger three islands, particularly given the substantial fluctuations expected for actual decay (as discussed in Sec. 4.2). The more significant discrepancy for the smallest island presumably

results from both fluctuations and an overestimation of the strength of the sink for diffusion atoms provided by the nearby extended step edge. In the vicinity of this smallest island, the extended step edge has a finite curvature, rather than the assumed near-zero curvature. Also, the analytic theory assumes that a strong sink (corresponding to a near straight step) surrounds the island, whereas the extended step is just on one side of the island.

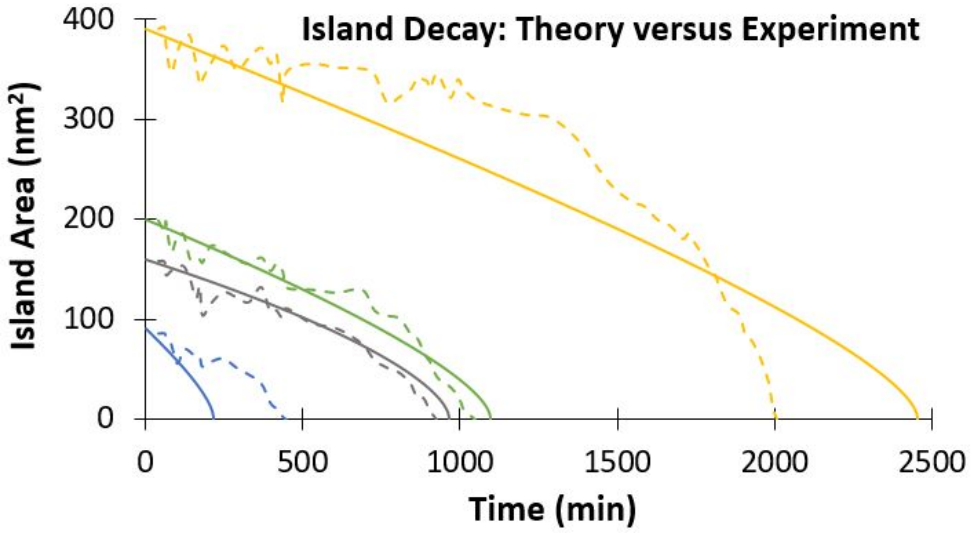

Figure 9. *Comparison between analytic results for island decay (solid line) and experiment (dashed line). The color of the line corresponds to the island in Fig.3 with the same color.*

For the second-layer island tracked in Fig.7 and Fig.8, $R(t)$ versus t was from numerical integration of Eq. 2 with the experimental initial size, $R(t=0) \approx 7.4$ nm, corresponding to an initial area $A(t = 0) = 170$ nm^2, and a supporting island with constant size corresponding to $R_S \approx$ 20 nm (i.e., the analytic treatment ignores the slight increase in radius of the supporting island during decay of the second layer island). Model parameters were selected as above, except that now the ES barrier must also be specified. We analyze behavior for four values in the range $\delta =$ 0.1078 to 0.1183 eV. The results shown in Fig.10 all exhibit non-linear decay similar to experiment. We suggest that an ES barrier of $\delta \approx 0.112$ eV best matches experiment. However, it should be emphasized that we expect large fluctuations in experimental behavior. (As an aside, analysis of second-layer island decay from the example in Fig.3 reveals unusually linear area decay, although perhaps just due to fluctuations, and an ES barrier estimate of $\delta \approx 0.13$ eV not much different from that above.) See Sec.4.2. An early semi-empirical EMT treatment gave $\delta =$ 0.16 eV for hopping over steps,[45] and a Tight Binding-SMA assessment produced $\delta = 0.18$ eV for exchange at A-steps and also for hopping over B-steps.[46]

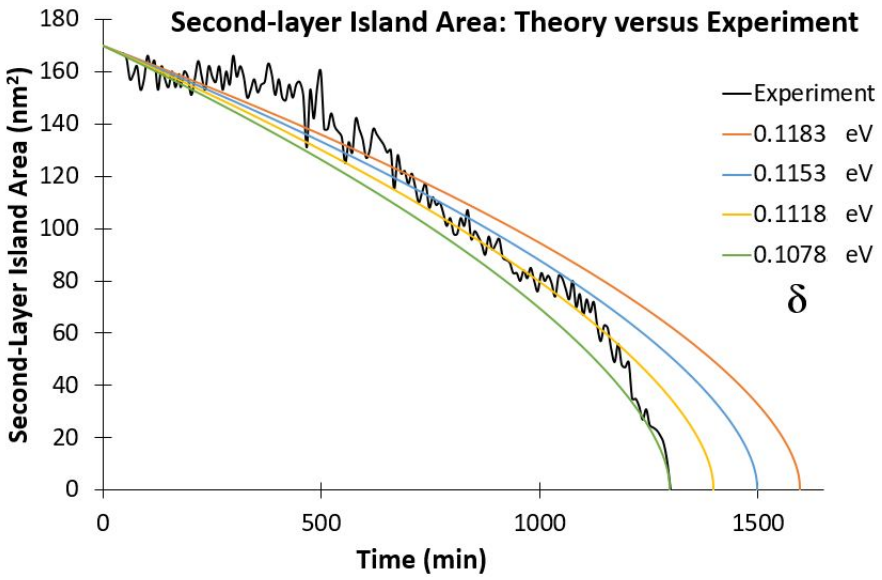

Figure 10. *Comparison between experimental second-layer island decay and analytic results using multiple ES barriers.*

4.2. KMC simulation of second-layer island decay

Experimental analysis of island decay cannot readily assess the extent fluctuations in the decay process, i.e., the variation in decay behavior if the experiment could be repeated multiple times starting from the same initial configuration. Likewise, the analytic theory presented above gives no insight into fluctuations since the prediction corresponds to behavior averaged over many stochastic decay processes. In this respect, KMC simulation of an appropriate stochastic model is ideal since one can repeat the "simulation experiment" for the same initial conditions. Thus, we perform simulations of the decay of a second-layer island analogous to the experimental configuration using the lattice-gas model described in Sec.2.3. For computational efficiency, we choose a smaller initial area of about $A(t=0) = 100$ nm^2 and also perform the simulations at 600 K (rather than 300 K). The stochastic model and its parameters are selected as described in Sec.2.3, and we also select an ES barrier of $\delta = 0.112$ eV corresponding to our estimate for Au on Au(111). We note that this value should be regarded as an effective barrier since it is likely that there exist different "local" ES barrier for different step orientations or local geometries.[30,32,46] Results shown in Fig.11 for 20 simulation trials indicate substantial fluctuations in $A(t)$ versus t. For comparison, the prediction of the analytic theory for the same parameters is also shown. Some difference from simulation behavior likely at least in part reflects the different island geometry.

A conclusion from this KMC analysis is that when comparing experimental results for island decay with predictions from the deterministic analytic theory (such as in Fig.9 or Fig.10), any assessment of consistency or otherwise should account for substantial fluctuations in the stochastic island decay process.

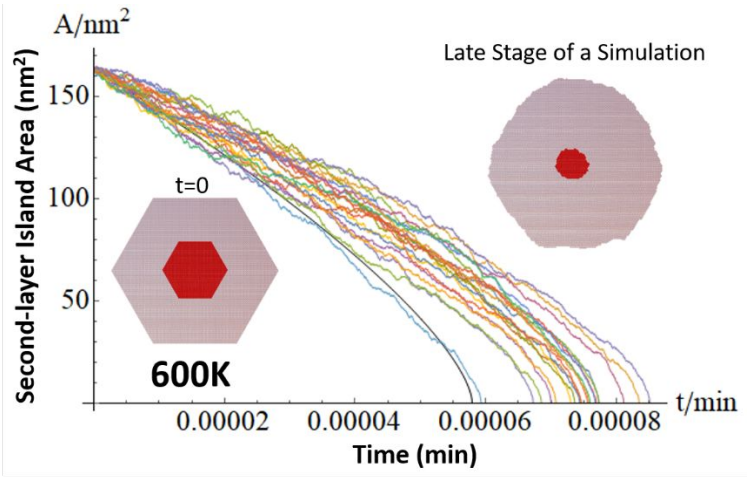

Figure 11. *KMC simulations results (20 trials) for second-layer island decay compared with analytical results (smooth black curve) both at 600 K. Inset: simulated island configurations at t=0 (lower left) and at a late stage of decay (upper right). Red atoms in the second-layer island, and purple atoms in the supporting island.*

5. COMPARISON OF BEHAVIOR FOR Au(111) WITH Ag(111) AND Cu(111)

It is natural to compare the rate of TD-limited OR for 2D Au islands on Au(111) with those for TD-limited OR on (111) surfaces of other coinage metals, Ag and Cu. As discussed, below observed difference in rates correlate with the different values of the effective barrier, E_{OR}, for OR, which are summarized in Table 1.

Au island decay on Au(111) is far slower than that of Ag islands on Ag(111). Morgenstern *et al.*[27] observed that a somewhat isolated a 113 nm^2 Ag islands decay within 21 minutes on Ag(111), while we observed a similar size Au island on Au(111), located next to a step edge took almost 500 minutes to decay. This difference in behavior is readily understood since the effective barrier, E_{OR}, for OR is much lower for Ag and for Au. Specifically for Ag on Ag(111), earlier DFT-PBE analysis predicted that E_d = 0.06 eV and E_{form} = 0.60 eV,[47] so that E_{OR}(Ag) = 0.66 eV which should be compared with E_{OR}(Au) = 0.91 eV reported in Sec.2.2. (The commonly used value of E_d = 0.10 eV for Ag on Ag(100) based on analysis of island formation during deposition is plausibly an overestimate since the modeling does not account for weak long-range oscillatory interactions between Ag adatoms.[48]) We also note an experimental estimate of E_{OR}(Ag) = 0.71 eV.[24]

Table 1. Energies controlling OR. Values for E_{OR} in parenthesis include the ES barrier as applies for second-layer island decay. a = Ref. 44, b = Ref. 32 (cf. Ref. 31), c = Ref. 47

values in eV	Au	Cu	Ag
ES barrier δ	0.11	0.12[a]	0.08 & 0.16[b]
terrace diff. E_d	0.12	0.05[c]	0.06[c]
formation en. E_{form}	0.79	0.82	0.60[c]
eff. OR barrier E_{OR}	0.91 (1.02)	0.87 (0.99)	0.66 (0.74-0.82)

Au island decay on Au(111) also appears to be somewhat slower than that of Cu islands on Cu(111). Icking-Konert *et al.*[44] observed that Cu islands with initial area around 300 nm^2 decayed within 12 hours. They also provided an experimental estimate of E_{OR} = 0.78 eV. An earlier DFT-PBE analysis predicted that E_d = 0.05 eV and E_{form} = 0.80 eV.[47] We repeated this analysis with the same settings as used in our DFT analysis for Au(111) (5×5 lateral unit cell, etc.) to recover the same value for E_d and a slightly higher value for E_{form} = 0.82 eV. These results indicate that E_{OR}(Cu) = 0.85-0.87 eV compared with E_{OR}(Au) = 0.91 eV, consistent with somewhat slower decay for Au islands on Au(111).

6. CONCLUSIONS

Our STM observations reveal very slow decay of Au islands on a Au(111) surface at 300 K (on the time scale of 10's of hours), consistent with previous observations of Peale *et al.* of very stable islands at 300 K.[34] Unlike this previous study, we have quantified the decay, and shown that it is consistent with predictions of analytical theory incorporating DFT values for the terrace diffusion barrier and the adatom formation energy, as well as an estimate of the step energy. We note again that our analysis ignores the herringbone reconstruction of Au(111), but evidently this reconstruction does not have a significant impact on coarsening processes on the length scale of 10's of nm. Coarsening of Au islands on Au(111) corresponds to TD-limited OR, just as for the analogous process on (111) surfaces of the other coinage metals, Ag and Cu. However, there is a difference in the coarsening rates.

From analysis of the decay of second-layer islands, we obtain an estimate for the ES barrier of $\delta \approx 0.11$ eV for Au on Au(111) from comparison of experimental and analytic theory. The analogous approach had been effectively used previously to assess the ES barrier for Ag on Ag(111).[31] We note that in making such comparisons, it is appropriate to be aware of substantial fluctuations in the decay process which we realize by KMC simulations of a suitable stochastic lattice-gas model for island decay.

AUTHOR INFORMATION

Corresponding Authors
*E-mail: evans@ameslab.gov (James W. Evans), pthiel@ameslab.gov (Patricia A. Thiel)

ORCID
King C. Lai: 0000-0003-2764-356X
Yong Han: 0000-0001-5404-0911
James W. Evans: 0000-0002-5806-3720
Patricia A. Thiel: 0000-0003-4195-0216

Notes
The authors declare no competing financial interest.

ACKNOWLEDGEMENTS

PS performed and PT supervised the experimental component of this work which was supported by NSF Grant CHE-1507223. KL performed the analytical modeling which was supported by the

U.S. Department of Energy (USDOE), Office of Science, Basic Energy Sciences, Division of Chemical Sciences, Geosciences, and Biosciences through the Ames Laboratory Chemical Physics program. Ames Laboratory which is operated for the USDOE by Iowa State University (ISU) under Contract No. DE-AC02-07CH11358. YH performed DFT analysis and JE supervised the theoretical studies supported by NSF Grant CHE-1507223. DFT calculations were mainly performed with the Extreme Science and Engineering Discovery Environment (XSEDE), which is supported by National Science Foundation under Grant No. ACI-1548562, and also partly used the computational resources at the National Energy Research Scientific Computing Centre (NERSC) supported by the USDOE Office of Science under Contract No. DE-AC02-05CH11231.

REFERENCES

(1) Ulman, A. Formation and structure of self-assembled monolayers. *Chem. Rev.* **1996**, *96*, 1533−1554.
(2) Love, J. C.; Estroff, L. A.; Kriebel, J. K.; Nuzzo, R. G.; Whitesides, G. M. Self-assembled monolayers of thiolates on metals as a form of nanotechnology. *Chem. Rev.* **2005**, *105*, 1103−1169.
(3) Vericat, C.; Vela, M. E.; Corthey, G.; Pensa, E.; Cortés, E.; Fonticelli, M. H.; Ibañez, F.; Benitez, G. E.; Carro, P.; Salvarezza, R. C. Self-assembled monolayers of thiolates on metals: a review article on sulfur-metal chemistry and surface structures. *RSC Adv.* **2014**, *4*, 27730−27754.
(4) Madix R. J.; Friend C. M. Interfacial chemistry: Gold's enigmatic surface. *Nature* **2011**, *479*, 482-483.
(5) Friend, C. M.; Hashmi S. A. K. Gold catalysis. *Accounts of Chemical Research* **2014**, *47*, 729–730.
(6) Biener, M. M.; Biener, J.; Friend, C. M. Sulfur-induced mobilization of Au surface atoms on Au(111) studied by real-time STM. *Surf. Sci.* **2007**, *601*, 1659–1667.
(7) Min, B. K.; Deng, X.; Pinnaduwage, D.; Schalek, R.; Friend, C. M. Oxygen-induced restructuring with release of gold atoms from Au (111). *Phys. Rev. B* **2005**, *72*, 121410.
(8) Mosier-Ross, P. A. Review of SERS Substrates for Chemical Sensing, *Nanomaterials (Basel)* **2017**, *7*, 142, 30 pp.
(9) S. A. Maier, M. L. Brongersma, P. G. Kiki, S. Meltzer, A. A. G. Requicha and H. A. Atwater, Plasmonics - A route to nanoscale optical devices. *Adv. Mater.*, **2001**, *13*, 1501-1505.
(10) Amendola, V.; Pilot, R.; Frasconi, M.; Maragò, O. M.; Iatì, M. A. Surface plasmon resonance in gold nanoparticles: a review. *J. Phys.: Cond. Matter*, **2017**, *29*, 203002, 48 p.
(11) Saha, K.; Agasti, S. S.; Kim, C.; Li, X.; Rotello, V. M. Gold nanoparticles in chemical and biological sensing. *Chem. Rev.*, **2012**, *112*, 2739-2779.
(12) Cabuzu, D.; Cirja, A.; Puiu, R.; Grumezescu, A. M. Biomedical applications of gold nanoparticles. *Curr. Top. Med. Chem.* **2015,** *15*, 1605-1613.
(13) Fortin, M. A.; Simao, T.; Laprise-Pelletier, M., Gold nanoparticles for imaging and cancer therapy. In *Nanooncology: Engineering Nanomaterials for Cancer Therapy and Diagnosis*, Goncalves, G.; Tobias, G., Eds. Springer International Publishing Ag: Cham, 2018; pp 1-50.
(14) Haruta, M.; Yamada, N.; Kobayashi, T.; Iijima, S. Gold catalysts prepared by co-precipitation for low-temperature oxidation of hydrogen and of carbon monoxide. *J. Catal.* **1989**, *115*, 301-309.
(15) Valden, M.; Lai, X.; Goodman, D. W. Onset of catalytic activity of gold clusters on titania with the appearance of nonmetallic properties. *Science*, **1998**, *281*, 1647-1650.
(16) Baletto, F.; Ferrando, R. Crossover among structural motifs in transition and noble-metal clusters. *J. Chem. Phys.* **2002**, *116*, 3856-3863.
(17) Garden, A. L.; Pedersen, A.; Jónsson, H. Reassignment of 'magic numbers' for Au clusters of decahedral and FCC structural motifs. *Nanoscale*, **2018**, *10*, 5124-5132.
(18) Cleveland, C. L.; Landman, U.; Shafigullin, M. N.; Stephens, P. W.; Whetten, R. L. Structural Evolution of Larger Gold Clusters. *Z. Phys. D: At., Mol. Clusters* **1997**, *40*, 503-508.

(19) Argyle, M. D.; Bartholomew, C. H. Heterogeneous Catalyst deactivation and regeneration: A review. *Catalysts* **2015,** *5*, 145-269.
(20) Xia, Y.; Xia, X.; Peng, H.-C. Shape-controlled synthesis of colloidal metal nanocrystals: Thermodynamic versus kinetic products. *J. Am. Chem. Soc.* **2015**, *137*, 7947−7966.
(21) Yuk, J. M.; Jeong, M.; Kim, S. Y.; Seo, H. K.; Kim, J.; Lee, J. Y. In situ atomic imaging of coalescence of Au nanoparticles on graphene: rotation and grain boundary migration. *Chem. Commun.* **2013**, *49*, 11479-11481.
(22) Lai, K. C.; Evans, J. W. Reshaping and sintering of 3D fcc metal nanoclusters: Stochastic atomistic modeling with realistic surface diffusion kinetics, *Phys. Rev. Materials* **2019**, *3*, 026001.
(23) Lai, K. C.; Han, Y.; Spurgeon, P. Huang, W.; Thiel, P. A.; Liu, D.-J.; Evans, J. W. Reshaping, intermixing, and coarsening of metallic nanocrystals: Non-equilibrium statistical mechanical and coarse-grained modeling. *Chem. Rev.* **2019**, *119*, 6670-6768.
(24) Morgenstern, K. Fast scanning tunnelling microscopy as a tool to understand changes on metal surfaces: from nanostructures to single atoms. *Phys. Status Solidi B* **2005**, *242*, 773-796.
(25) Thiel, P. A.; Shen, M.; Liu, D.-J.; Evans, J. W. Coarsening of two-dimensional nanoclusters on metal surfaces. *J. Phys. Chem. C* **2009**, *113*, 5047-5067.
(26) Giessen, M. Step and island dynamics at solid/vacuum and solid/liquid interfaces. *Prog. Surf. Sci.* **2001**, *68*, 1-153.
(27) Morgenstern, K.; Rosenfeld, G.; Comsa, G., Decay of two-dimensional Ag islands on Ag(111). *Phys. Rev. Lett.* **1996,** 76, 2113-2116.
(28) Han, Y.; Russell, S. M.; Layson, A. R.; Walen, H.; Yuen, C. D.; Thiel, P. A.; Evans, J. W., Anisotropic coarsening: One-dimensional decay of Ag islands on Ag(110). *Phys. Rev. B* **2013,** 87, 155420.
(29) Michely. T.; J. Krug, J. Islands, mounds, and atoms, Springer, Berlin, 2004.
(30) Evans, J. W.; Thiel, P. A.; Bartelt, M. C. Morphological evolution during epitaxial thin film growth: Formation of 2D islands and 3D mounds. *Surf. Sci. Rep.* **2006**, *61*, 1-128.
(31) Morgenstern, K.; Rosenfeld, G.; Lægsgaard, E.; Besenbacher, F.; Comsa, G. Measurement of energies controlling ripening and annealing on metal surfaces, *Phys. Rev. Lett.* **1998**, *80*, 556-559.
(32) Li, M.; Chung, P.-W.; Cox, E.; Jenks, C. J.; Thiel, P. A.; Evans, J. W. Exploration of complex multilayer film growth morphologies: STM analysis and predictive atomistic modeling for Ag on Ag(111), *Phys. Rev. B*, **2008**, *77*, 033402.
(33) Jaklevic, R. C.; Elie, L. Scanning-tunneling-microscope observation of surface diffusion on an atomic scale: Au on Au(111). *Phys. Rev. Lett.* **1988**, *60*, 120-123.
(34) Peale, D. R.; Cooper, B. H., Adsorbate-promoted mass-flow on the gold(111) surface observed by scanning tunneling microscopy. *J. Vac. Sci. Technol. A-Vac. Surf. Films* **1992,** *10*, 2210-2215.
(35) Thiel, P. A.; Shen, M. M.; Liu, D. J.; Evans, J. W., Adsorbate-enhanced transport of metals on metal surfaces: Oxygen and sulfur on coinage metals. *J. Vac. Sci. Technol. A* **2010,** 28, 1285-1298.
(36) Nan, L.; Allan, D.; Gang-Yu, L. In situ STM study of thermal annealing of Au thin films: An investigation on decay of nanometer Au clusters and 2D islands. Acta Phys. Sinica (Overseas Edn) 1997, 6, 531-549.
(37) Walen, H.; Liu, D. J.; Oh, J.; Lim, H.; Evans, J. W.; Kim, Y.; Thiel, P. A., Self-organization of S adatoms on Au(111): √3R30° rows at low coverage. *J. Chem. Phys.* **2015,** *143*, 014704.
(38) Zinke-Allmang, M.; Feldman, L. C.; Grabow, M. H. Clustering on surfaces, *Surf. Sci. Rep.* **1992**, *16*, 377-463.
(39) Hausser, F.; Voigt, A., Ostwald ripening of two-dimensional homoepitaxial islands. *Phys. Rev. B* **2005,** *72*, 035437.
(40) Kim, S. Y.; Lee, I. H.; Jun, S., Transition-pathway models of atomic diffusion on fcc metal surfaces. I. Flat surfaces. *Phys. Rev. B* **2007,** 76, 245407.
(41) Mortenson, J. J.; Hammer, B.; Nielsen, O. H.; Jacobsen, K. W.; Norskov, J. K. DFT study of self-diffusion on the (111) surfaces of Ni, Pd, Pt, Cu, Ag and Au, pp 173-182 in Springer Series in Solid-State Sciences Vol. 121, Eds A. Okiji, H. Kasai, and K. Makoshi, Springer-Verlag, Berlin, 1996.

(42) Roling, L. T.; Mavrikakis, M. Toward rational nanoparticle synthesis: predicting surface intermixing in bimetallic alloy nanocatalysts, *Nanoscale*, **2017**, *9*, 15005-15017.
(43) Antczak, G.; Ehrlich, G. Surface diffusion: Metals, metal atoms, and clusters. Cambridge University Press, Cambridge, 2010.
(44) Icking-Konert, G. S.; Giesen, M.; Ibach, H., Decay of Cu adatom islands on Cu(111). *Surf. Sci.* **1998,** *398*, 37-48.
(45) Stoltze, P. Simulation of surface defects. *J. Phys.: Condens. Matter* **1994**, *6*, 9495-9517.
(46) Kim, S. Y.; Lee, I. H.; Jun, S., Transition-pathway models of atomic diffusion on fcc metal surfaces. II. Stepped surfaces. *Phys. Rev. B* **2007,** 76, 245408.
(47) Liu, D.-J. Density functional analysis of key energetics in metal homoepitaxy: Quantum size effects in periodic slab calculations. *Phys. Rev. B* **2010**, *81*, 035415.
(48) Fichthorn, K. A.; Scheffler, M. Island nucleation in thin-film epitaxy: A first-principles study, *Phys. Rev. Lett.* **2000**, *84*, 5371-5374.

TOC IMAGE

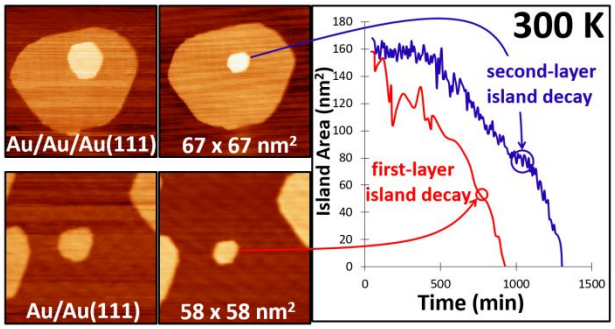
Au/Au/Au(111)
67 x 67 nm²
Au/Au(111)
58 x 58 nm²
300 K
second-layer
island decay
first-layer
island decay
Island Area (nm²)
Time (min)
0
20
40
60
80
100
120
140
160
180
0
500
1000
1500

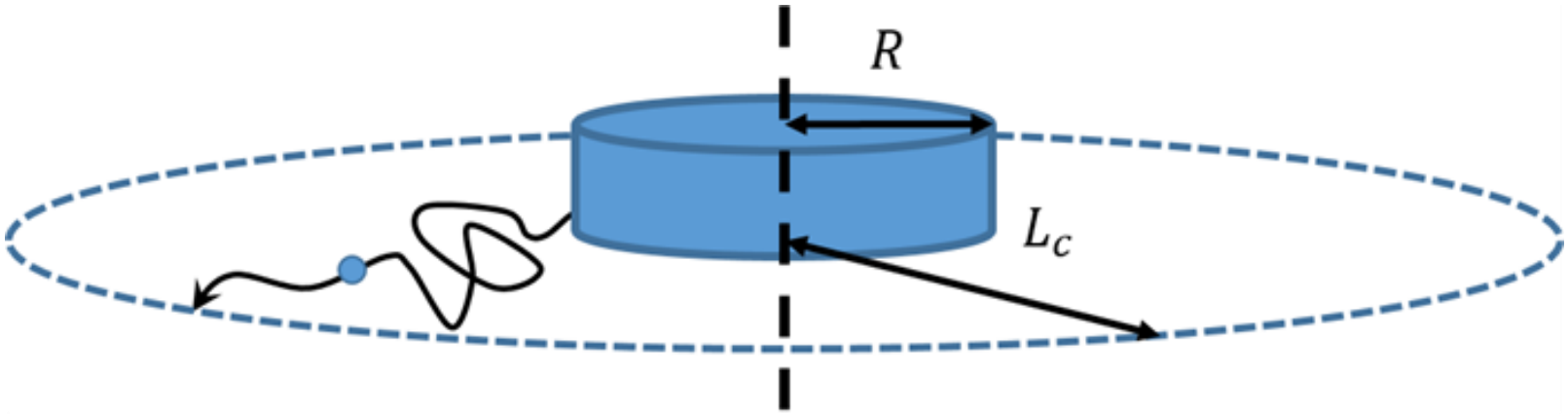
R
L_c

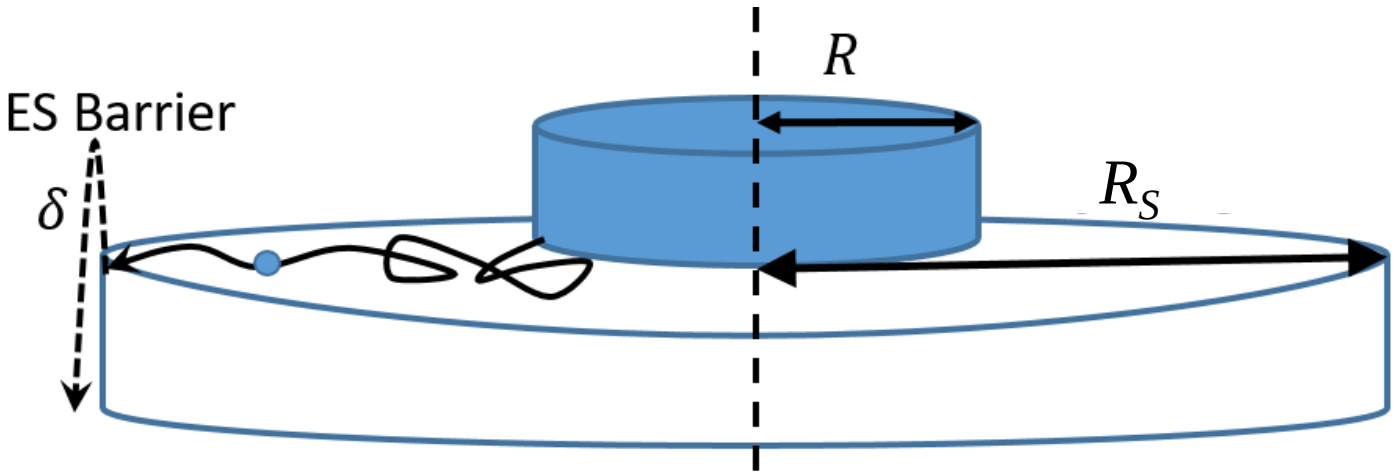
ES Barrier
δ
R
R_S

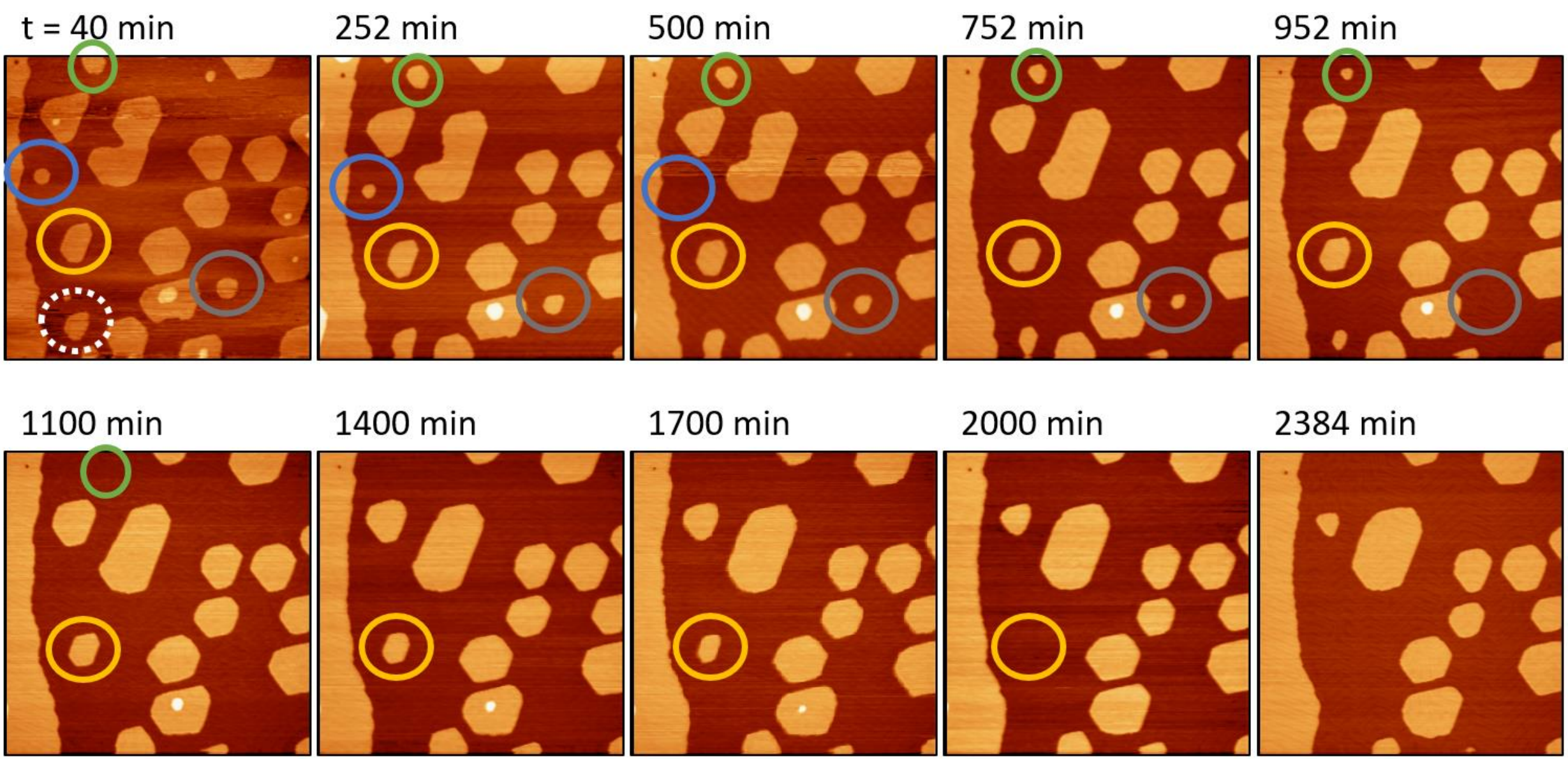
t = 40 min
252 min
500 min
752 min
952 min
1100 min
1400 min
1700 min
2000 min
2384 min

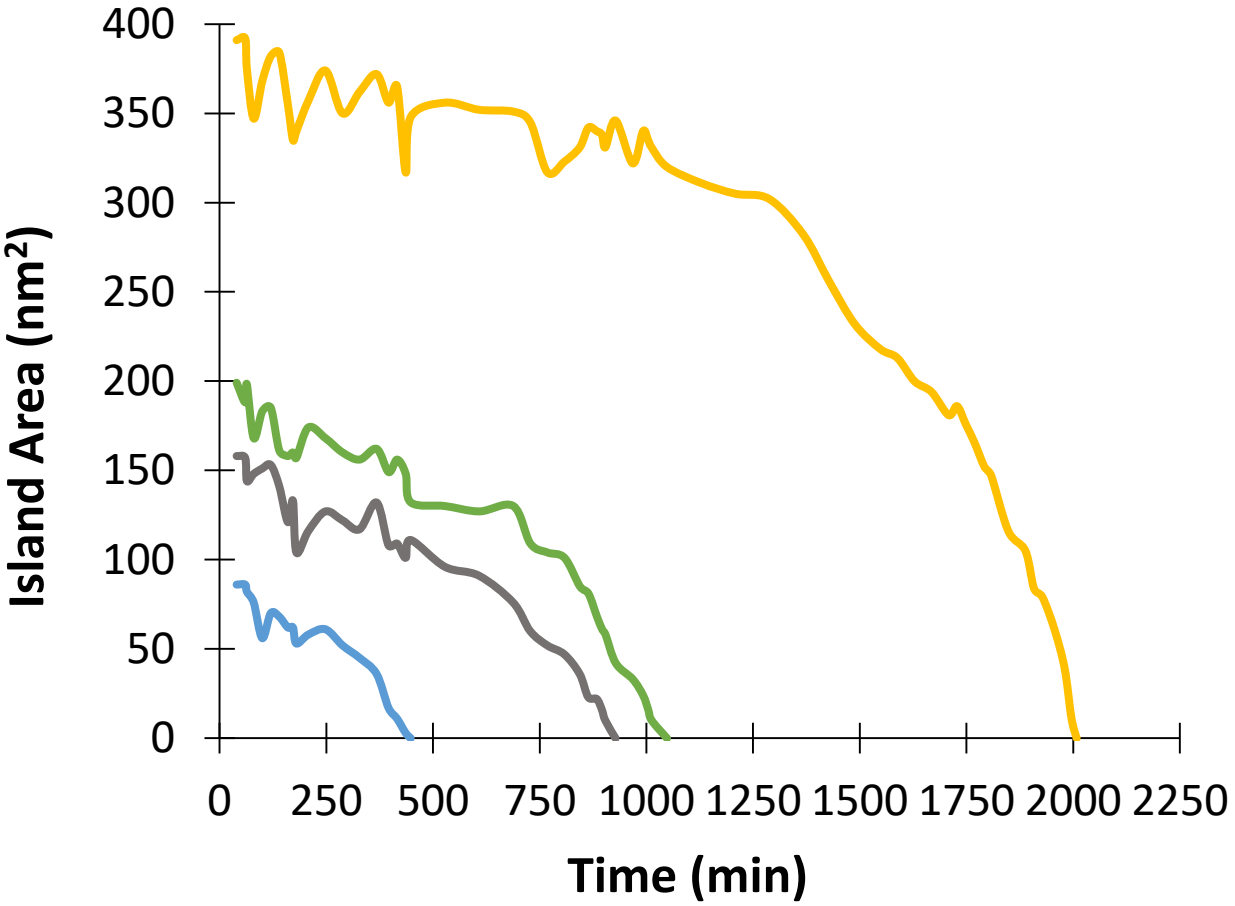
Island Area (nm²)
400
350
300
250
200
150
100
50
0
0
250
500
750
1000
1250
1500
1750
2000
2250
Time (min)

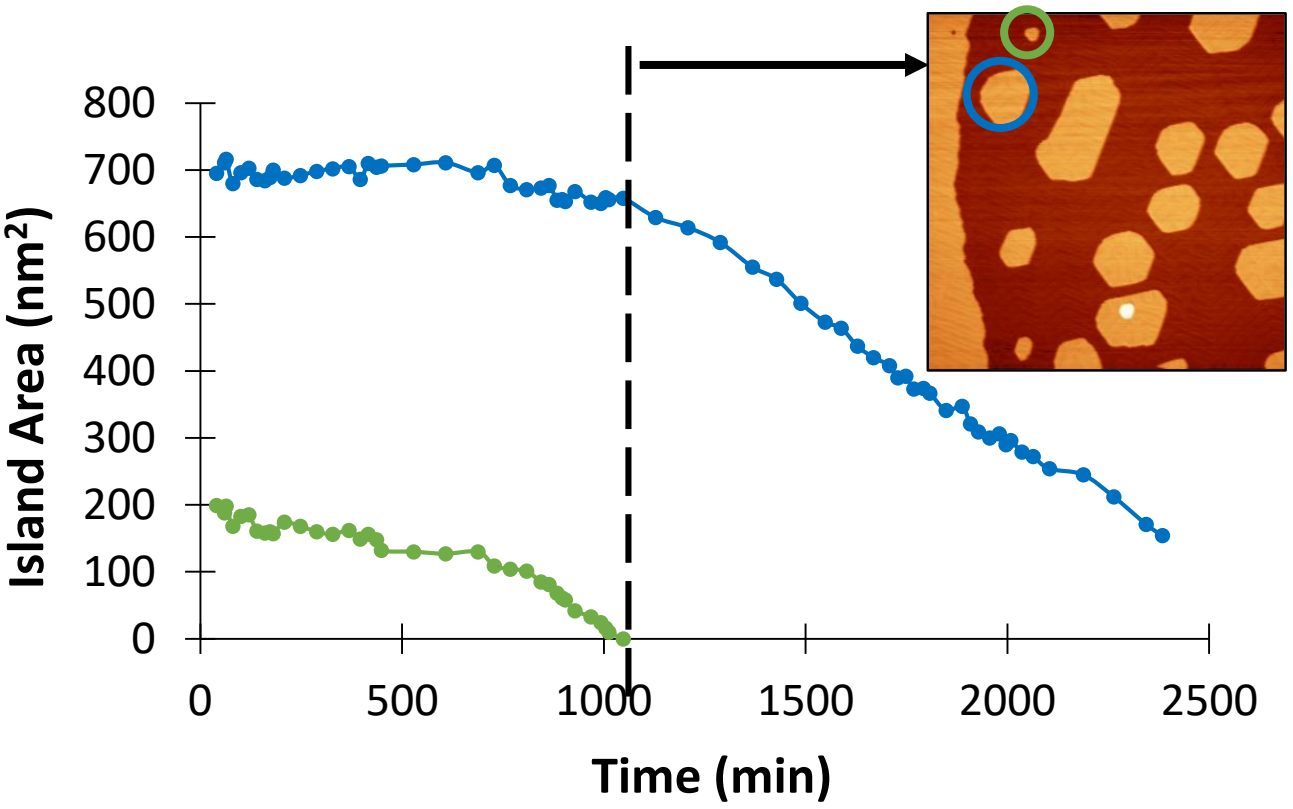
Island Area (nm²)
800
700
600
500
400
300
200
100
0
0
500
1000
1500
2000
2500
Time (min)

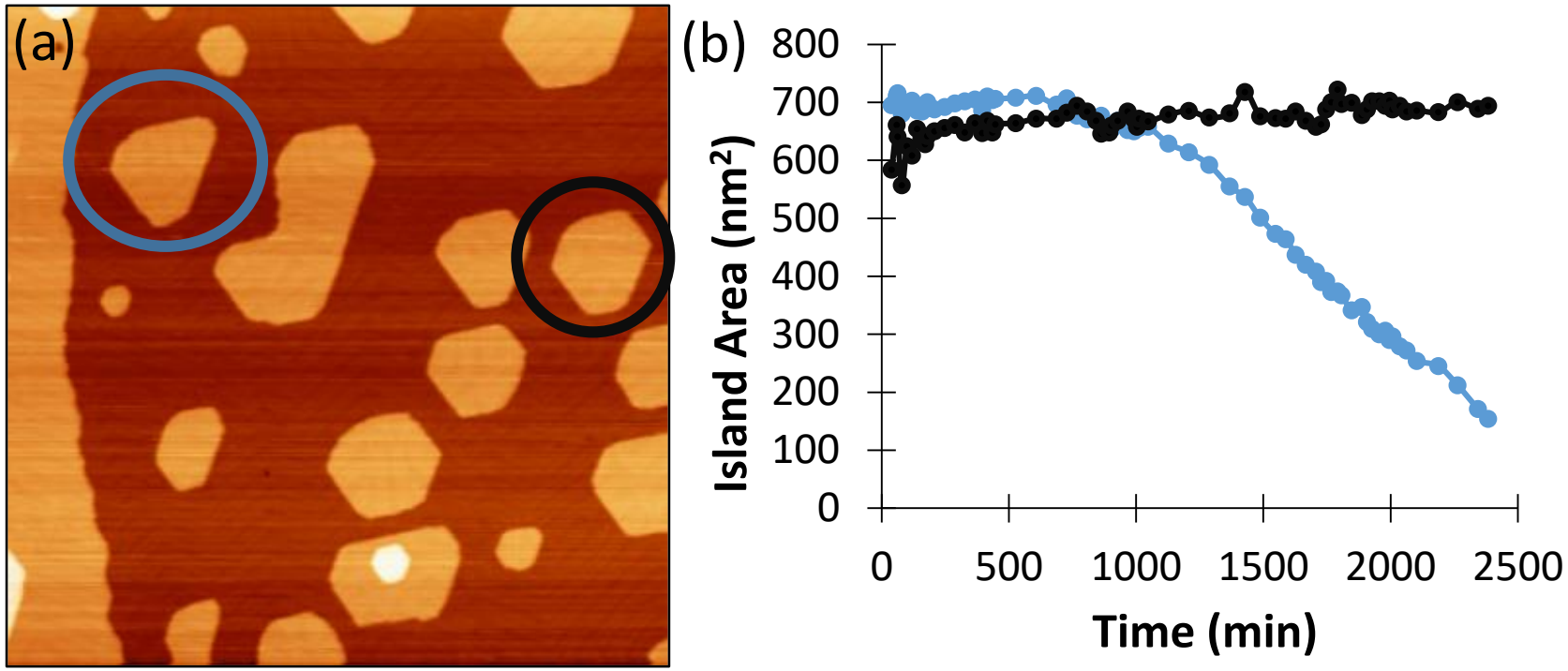
(a)
(b)
Island Area (nm²)
800
700
600
500
400
300
200
100
0
0
500
1000
1500
2000
2500
Time (min)

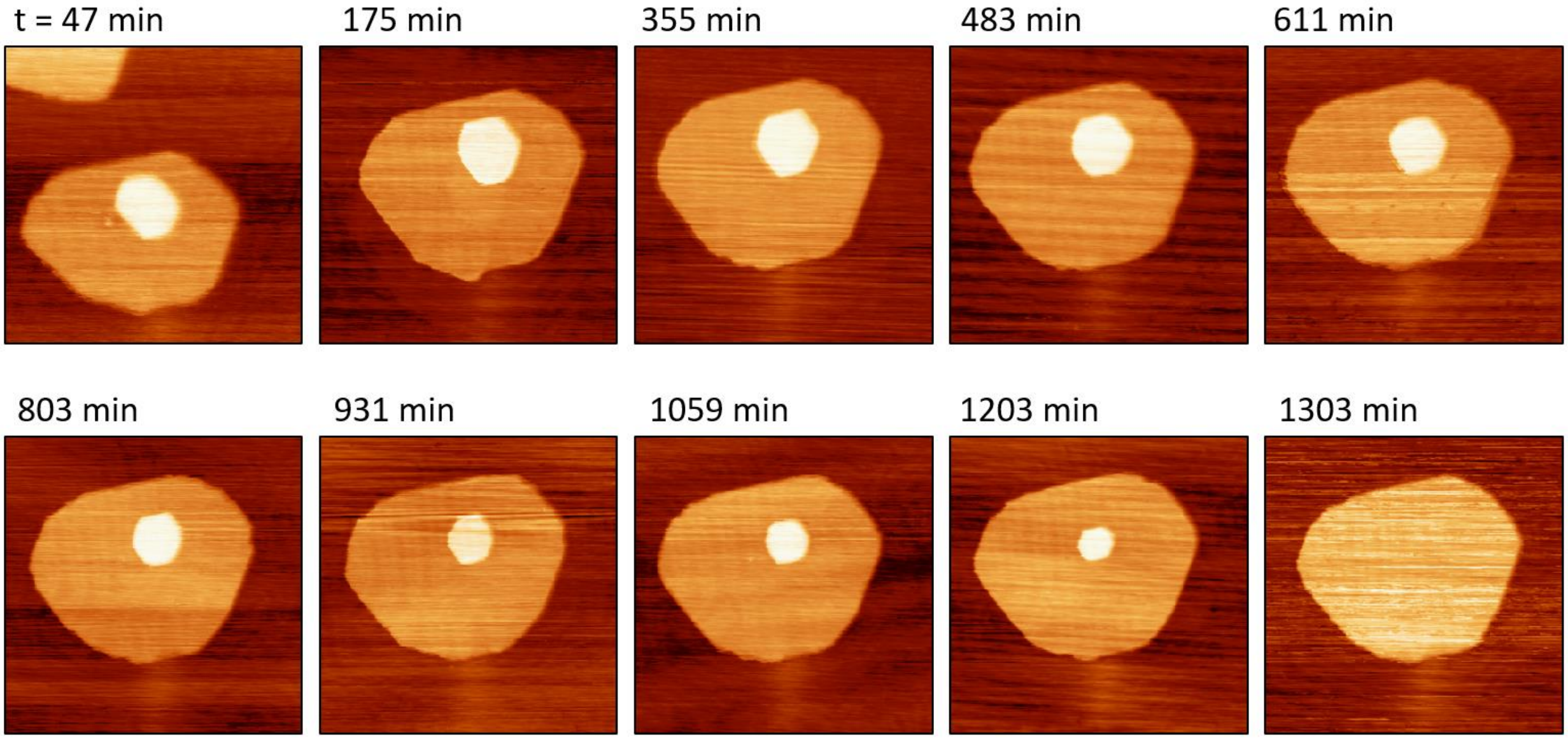
t = 47 min
175 min
355 min
483 min
611 min
803 min
931 min
1059 min
1203 min
1303 min

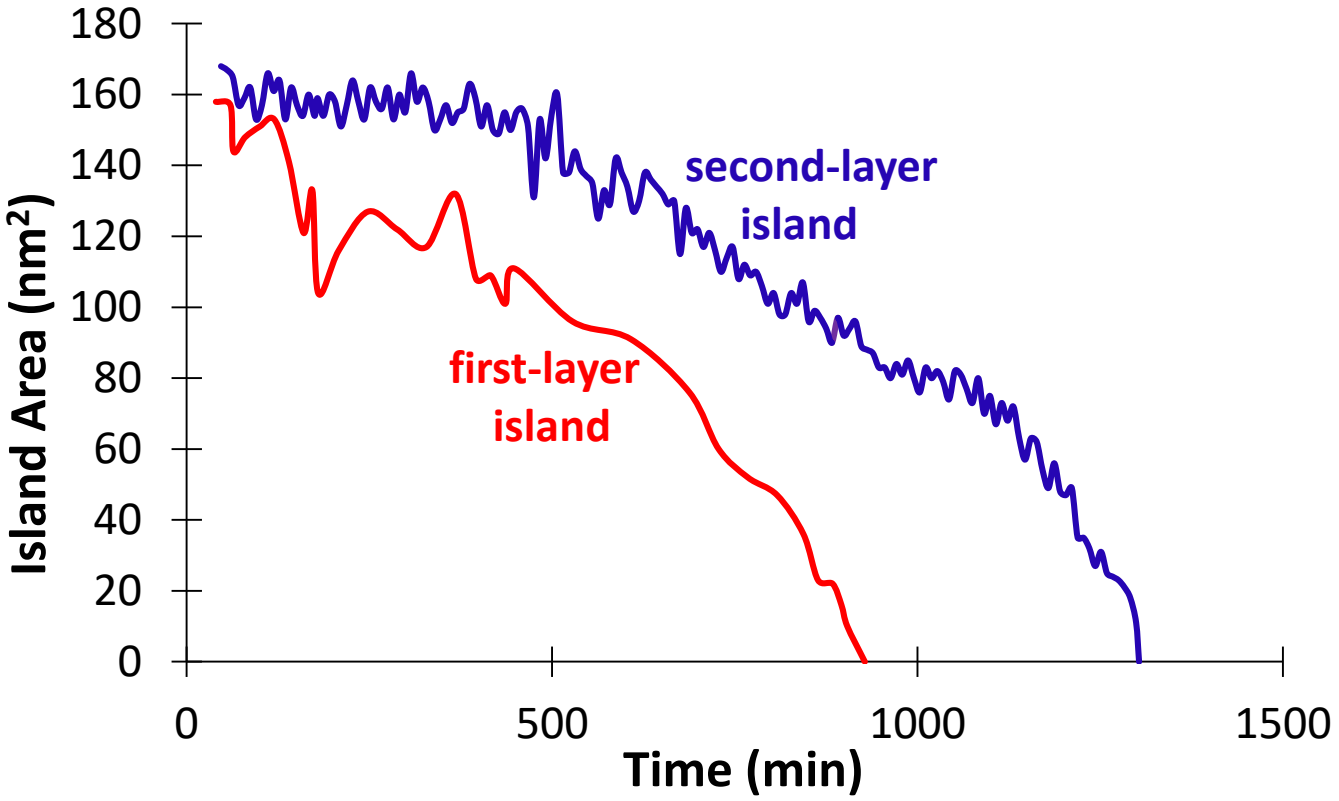
Island Area (nm²)
180
160
140
120
100
80
60
40
20
0
0
500
1000
1500
Time (min)
second-layer island
first-layer island

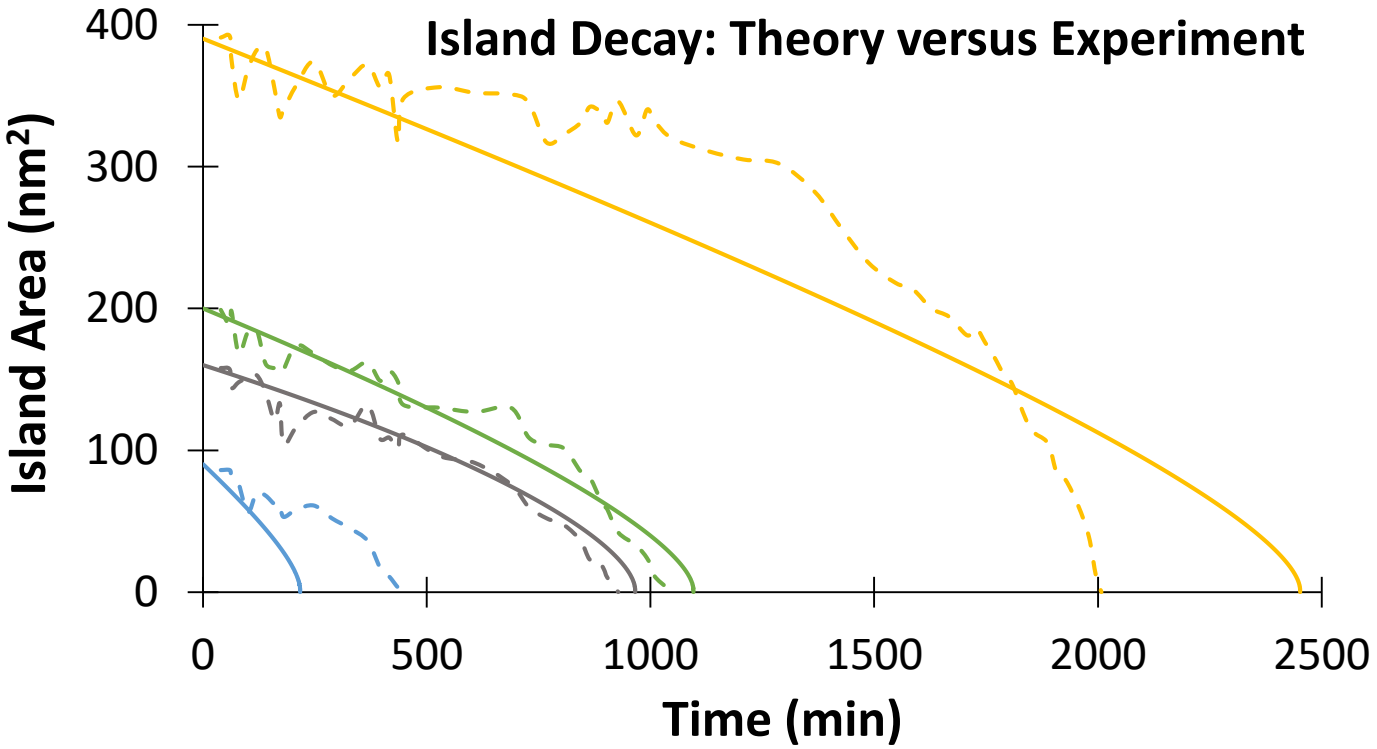
Island Decay: Theory versus Experiment
Island Area (nm²)
400
300
200
100
0
0
500
1000
1500
2000
2500
Time (min)

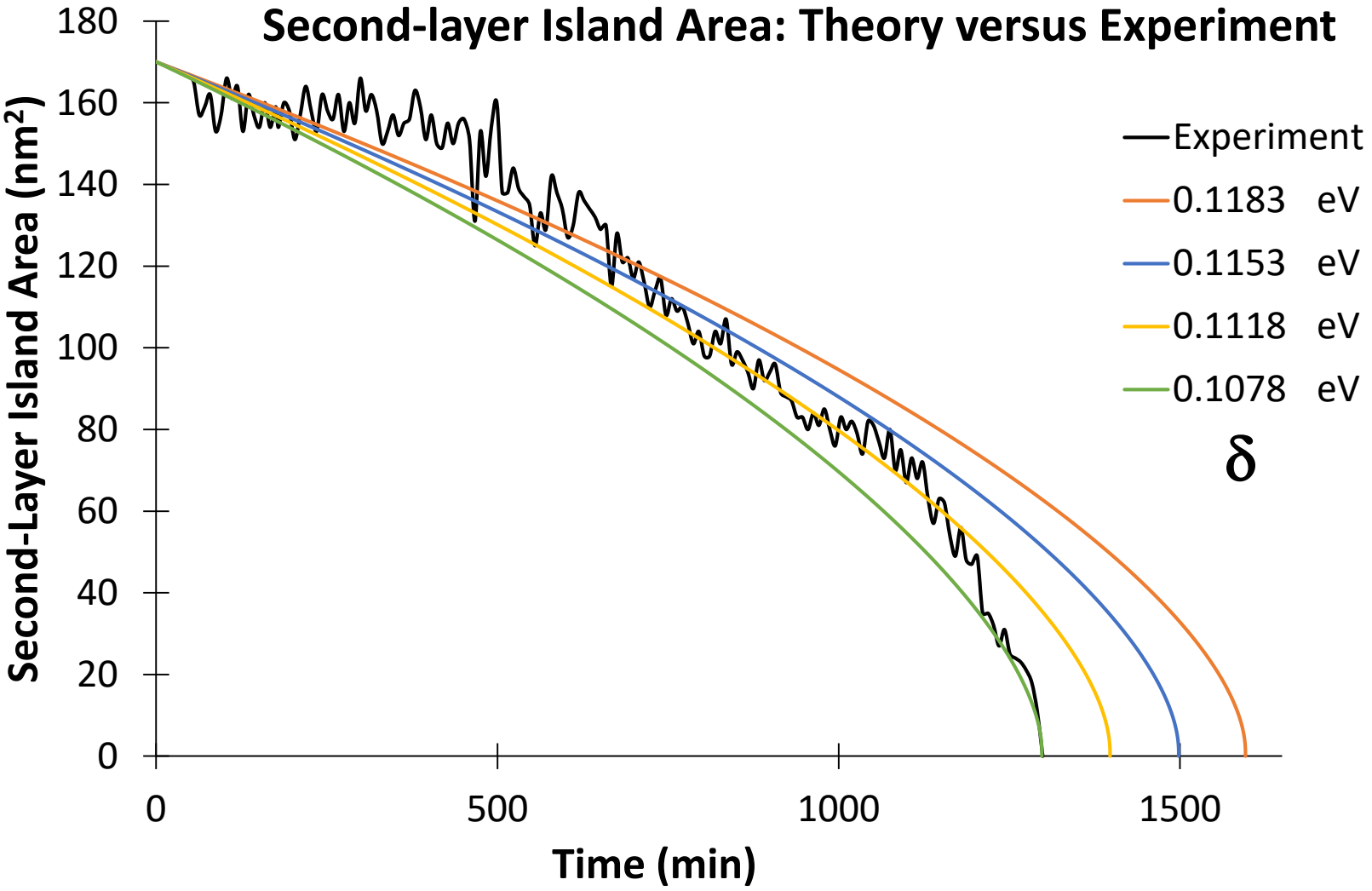
Second-layer Island Area: Theory versus Experiment
Second-Layer Island Area (nm²)
180
160
140
120
100
80
60
40
20
0
0
500
1000
1500
Time (min)
Experiment
0.1183 eV
0.1153 eV
0.1118 eV
0.1078 eV
δ

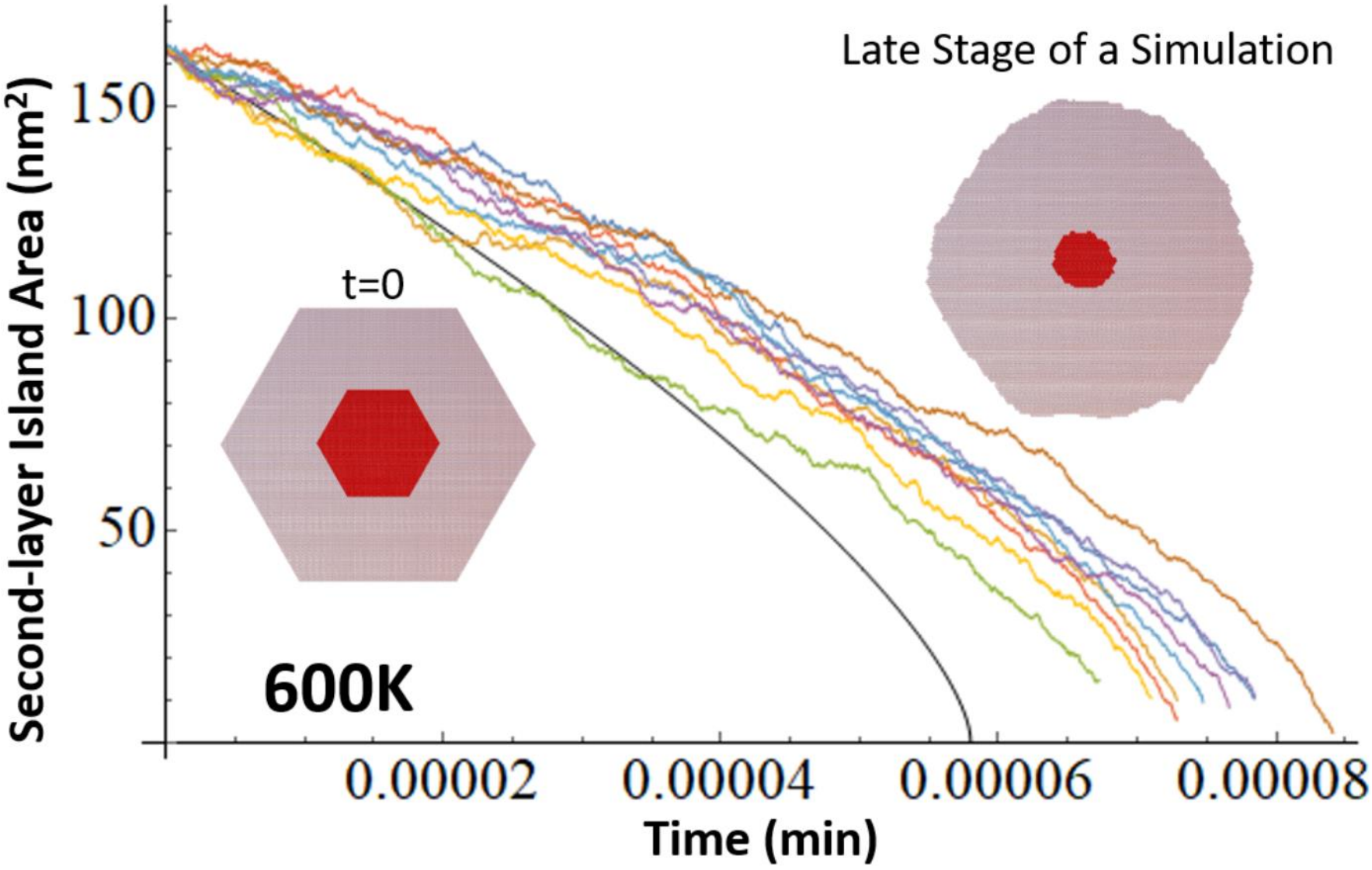
Late Stage of a Simulation
Second-layer Island Area (nm²)
150
100
50
t=0
600K
0.00002
0.00004
0.00006
0.00008
Time (min)